# The $CO_2$ Gas Cherenkov Detectors for the Jefferson Lab Hall–A Spectrometers

M. Iodice [a,1], E. Cisbani [a], S. Colilli [a], R. Crateri [a], S. Frullani [a], F. Garibaldi [a], F. Giuliani [a], M. Gricia [a], M. Lucentini [a], A. Mostarda [a], L. Pierangeli [a], F. Santavenere [a], G. M. Urciuoli [a], R. De Leo [b], L. Lagamba [b], A. Leone [c], R. Perrino [c], S. Kerohas [d], P. Vernin [d]

[a] *Physics Laboratory, Istituto Superiore di Sanità and Sezione INFN Sanità, viale Regina Elena 299, I-00161 Roma, Italy*

[b] *Dipartimento Interateneo di Fisica e Sezione INFN Bari, via Amendola 173, I-70126 Bari, Italy*

[c] *INFN Sezione di Lecce, via Arnesano, I-73100 Lecce, Italy*

[d] *CEA - Saclay, France*

**Abstract**

Two threshold gas Cherenkov counters have been constructed for the electron and hadron High Resolution Spectrometers (HRS) of the Jefferson Lab Experimental Hall–A. These counters are intended to separate electrons/positrons from other particles up to 4 GeV/c. The counters are operated at atmospheric pressure with $CO_2$. Each counter is equipped with ten mirrors. Light weight, thin spherical mirrors ($\sim 5.5 \times 10^{-3}$ radiation lengths) have been employed resulting in a total thickness of $\sim 1.4 \times 10^{-2}$ radiation lengths crossed by the particles. A prototype of the counter has been tested at CERN with a mixed beam of positrons, pions and protons from 1 to 4 GeV/c. Its detection efficiency for positrons and the rejection ratios for pions and protons have been measured as a function of the pulse height response (or equivalently the number of photoelectrons). An improvement of 34% in the number of photoelectrons has been obtained by using a wavelength shifter coated on the photocathode glass window.

With such an improvement in 1 m long radiator, an inefficiency for positrons less than $10^{-3}$ and rejection ratios $\pi/e$ at the level of few $10^{-3}$ and $p/e$ smaller than $10^{-3}$ have been obtained for pulse heights above 2 photoelectrons. Contaminations of particles below the Cherenkov threshold is fully understood considering $\delta$-rays production.

[1] Corresponding author. E-mail: mauro@axiss.iss.infn.it, fax: +39 6 4462872

## 1 Introduction

An accelerator for electrons in the "multi-GeV" region, (the Continuous Electron Beam Accelerator Facility - CEBAF), the first dedicated to Nuclear Physics, has recently become operational at Jefferson Lab. The accelerator configuration allows three countinuous beams to be delivered simultaneously to three experimental halls. Each hall is equipped with complementary sets of detectors and can use, partially independently from the others, electron beams with energy up to 4 GeV (and in a near future up to 6 GeV) and intensity up to 200 $\mu$A [1]. The experimental Hall–A is dedicated to high luminosity and high resolution studies of inclusive and semi-exclusive electron scattering reactions. This Hall is equipped with two identical, focusing magnetic High Resolution Spectrometers (HRS) able to detect charged particles with momenta up to 4 GeV/c. It is therefore well suited to carry out scattering experiments with the detection in the final state of the scattered electron (in the electron arm) in coincidence with a particle knocked-out from the target (a proton, a meson $\pi$, k, ..., in the hadron arm).

The detector system of each arm is positioned at the level of the focal plane, at the exit of the spectrometer; it allows the measurement of the momentum (through tracking detectors) and the identification of the particles: electrons (and positrons), pions, kaons, protons and eventually deuterons. This goal is achieved, both in the electron arm and in the hadron arm, by combining the information coming from a silica aerogel Cherenkov counter [2,3], a gas Cherenkov counter (subject of the present paper), the time of flight (TOF) between two planes of scintillators, an electromagnetic shower counter (only in the electron arm) [4], and, for experiments in coincidence, the coincidence time between the two spectrometers. In Fig. 1 the focal plane detector package for the hadron arm is shown.

The combination between the electromagnetic shower counter and the gas Cherenkov counter, in the electron arm, should allow to reach a rejection ratio between electrons and pions as high as $10^5$, a value that is required in particular kinematical conditions [1].

Each gas Cherenkov detector (one per each spectrometer) is operated at atmospheric pressure with $CO_2$, it is equipped with thin mirrors built at our laboratories and has an entrance area of about 2 m$^2$. The $CO_2$ radiator length is 1 m for the hadron arm, and 1.5 m for the electron arm. In the following we will refer to either of the detectors, if not otherwise specified.

A prototype has been also built in order to investigate in details the performances of the final detector.

In this paper we discuss details concerning the design and construction of

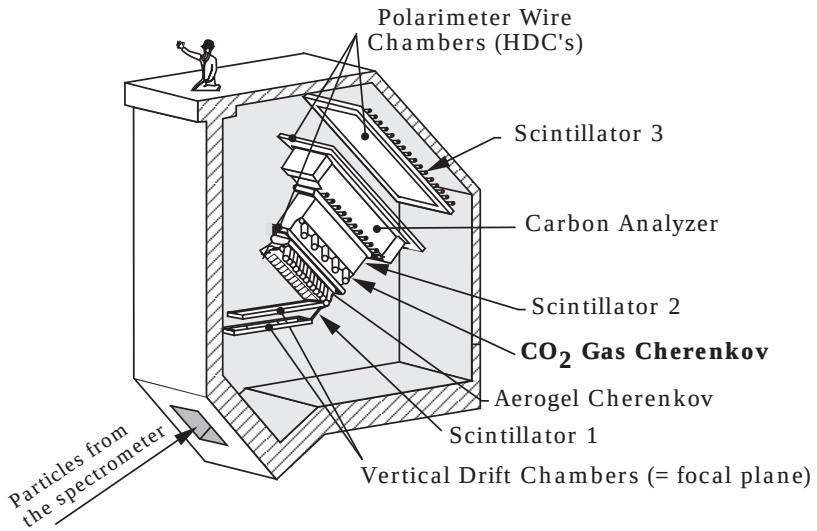


Fig. 1. The focal plane detector assembly of the High Resolution Spectrometer.

the counters and the performances of the prototype, as determined from the experimental tests performed at CERN with a mixed beam of positrons, pions and protons from 1 to 4 GeV/c.

## 2 General characteristics.

The requirement to distinguish electrons (or positrons, depending on the selected charge of the particles) from the hadron component ($\pi$, p, ...) in the whole range of momenta measurable with the HRS spectrometers, from 0.3 to 4 GeV/c, is completely fulfilled by a threshold Cherenkov counter with $CO_2$ gas as radiator. Its index of refraction at STP is $n = 1.00041$ (at the Sodium D line). Since only particles with $\beta > 1/n$ can produce Cherenkov radiation, the momentum threshold for electrons is sufficiently low, at 0.017 GeV/c, while the thresholds for pions and protons are above the HRS range, at 4.8 and 32 GeV/c, respectively. Detection of Cherenkov radiation, for any momentum measurable in HRS, could thus be used either as a tag for electrons, or as a veto for the identification of the heavier hadron component. This fast information can be also used for online trigger purposes.

### *2.1 The geometrical design of the detector.*

In order to characterize the geometrical layout of the detector, a preliminary study of the possible trajectories coming out from the spectrometers has been carried out through the codes RAYTRACE [5] and SNAKE [6]. Generating random rays covering the full acceptances in angles and momenta of the HRS,

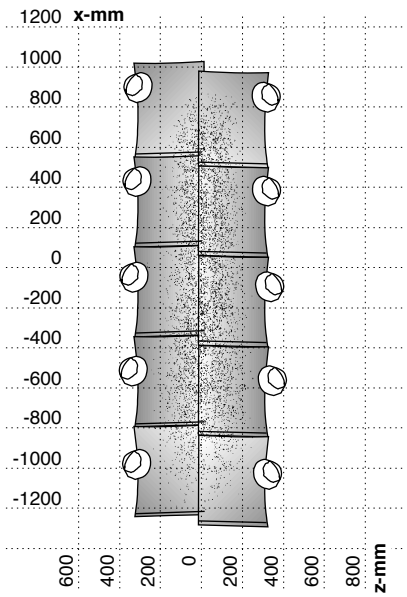


Fig. 2. Front view of Cherenkov light rays envelope at their impact onto the mirrors. Also the photocathodes (small circles) and mu-metal ends (large circle) are drawn.

and taking into account the extension of the target, these codes trace the particles through the magnetic elements of the spectrometer, to the focal plane detection package, resulting in the full envelope of trajectories crossing the gas Cherenkov detector over an area of about 0.8 $m^2$ with angle divergences up to 20 degrees. The study of the design of the detector has then been carried out taking advantage of dedicated Monte Carlo simulations for particles producing Cherenkov radiation [7], where the emitted photons are traced through their reflections on the mirrors to the photomultiplier tubes. Different configurations (length of the radiator, number of subsections, shape of the mirrors) have been considered.

The actual design consists in a 1.5 m (1 m) long detector in the direction of the central crossing particles for the electron (hadron) HRS arm with a $250\times80$ $cm^2$ wide surface perpendicular to that direction. The Cherenkov light is collected by ten spherical mirrors and focussed on ten photomultiplier (PM) tubes with 5" diameter (about 11 cm diameter photocathode sensitive surface). Fig. 2 shows the cross section of the envelope of the light rays as generated by the Monte Carlo at their impact on the mirrors. Upstream with respect to the mirrors, on the right and left sides of the figure, the positions occupied by the photocathode and mu-metal shieldings are also visible. Fig. 3 shows the front view and a 3-D drawing of the detector design.

The mirrors placed on two parallel rows, suitably tilted to reflect the light towards the PM's, have a spherical shape with a radius of curvature R=90 cm. The PM's are placed at a distance close to R/2=45 cm from the mirrors, where the parallel rays of light incident on the mirrors are approximately fo-

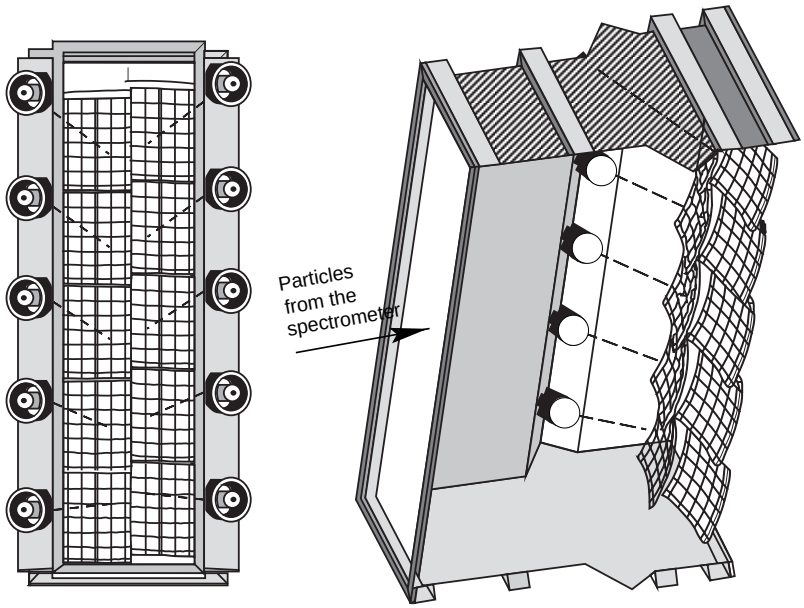


Fig. 3. Front view and "3-D", partially open, view of the Gas Cherenkov Detector.

cussed. The actual positions and angles of each individual PM were optimized according to the (expected) spectrometer emittance, in order to keep the reflected Cherenkov photons in a small spot at the center of the photocathode and perpendicular to it. To avoid "dark zones" between two adjacent mirrors, these partially overlap. Their shape is obtained by cutting a spherical shell by a parallelepiped whose cross section is a rectangle of dimensions $38 \times 48$ cm$^2$. Moreover, to prevent light losses in the overlapping zone between two adjacent mirrors, (hitting the mirror along its side edge), the cuts along the edges of the mirrors are suitably tilted, as given from the simulation.

From the knowledge of the optical magnetic properties of the spectrometers, the Monte Carlo (MC) simulations led us to a geometrical design of the detector where all the photons emitted in the radiator are collected on the central part of the photomultipliers, after reflections on the mirrors. As an example we report in Fig. 4 the MC results obtained for the particles crossing the two mirrors in the bottom part (with respect to Fig. 2) of the detector. This is the worst case, since the rays are more inclined than in other regions of the spectrometer. The figure clearly shows that all the photons hitting the two mirrors (see the top-right part of Fig. 4) are well focussed on the associated PM's (see the top-left part in Fig. 4).

### *2.2 Expected detector response.*

Besides the geometry, the choice and the characterization of the materials have to be investigated in order to optimize the response of the detector. The

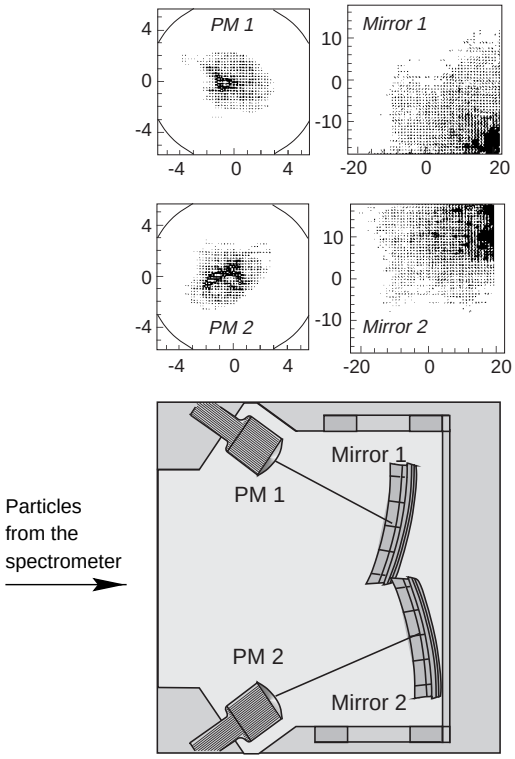


Fig. 4. Envelope on the mirrors of the produced Cherenkov radiation (top-right) and its image onto the photomultipliers (top-left).

number of photoelectrons ($p.e.$) emitted in a wavelength range from $\lambda_1$ to $\lambda_2$ is given by:

$$N_{p.e.} = 2\pi\alpha\, L \int_{\lambda_1}^{\lambda_2} QE(\lambda)\, \varepsilon_{coll}(\lambda)\, \frac{1}{\lambda^2}\, \sin^2\vartheta_C(\lambda)\, d\lambda \qquad (1)$$

where $\alpha$ is the fine-structure constant, $L$ is the path length in the radiator, $\varepsilon_{coll}$ is the efficiency for collecting the Cherenkov light, $QE(\lambda)$ is the quantum efficiency of the photomultiplier, and

$$\sin^2\vartheta_C(\lambda) = 1 - \frac{1}{n^2(\lambda)\beta^2}$$

being $\vartheta_C$ the polar angle of the emitted Cherenkov photons with respect to the direction of the incident particle, $n$ the index of refraction of the radiator and $\beta$ the velocity of the particle in c units

When no Cherenkov photons are lost for geometrical reasons and when Rayleigh scattering is included in the transmittivity $T(\lambda)$ of the radiator, the collection efficiency curve can be obtained from the product of the transmittivity curve

and a mirror reflectivity $R(\lambda)$:

$$\varepsilon_{coll}(\lambda) = T(\lambda)\, R(\lambda)$$

In typical Cherenkov detectors, the index of refraction of the radiator is nearly constant over the useful $\lambda$ range of photocathode sensitivity. In this case,

$$N_{p.e.} = L N_0 < \sin^2 \vartheta_C(\lambda) > \tag{2}$$

where

$$N_0 = 2\pi\alpha \int_{\lambda_1}^{\lambda_2} QE(\lambda)\, T(\lambda)\, R(\lambda)\, \frac{1}{\lambda^2}\, d\lambda$$

is the figure of merit of the detector which should be maximized.

## 3 Construction of the detector

### *3.1 Mechanics*

The external structure of the two detectors have been built with 2.5 mm thick folded welded steel. The entrance and exit windows are made of Tedlar foils (Polyvinyl fluoride, $2 \times 37.5\mu$m thick film per window), a very thin and highly opaque material. The composition and the high tensile and tear strengths, inertness and thermal stability properties of Tedlar, combine to make an excellent film to match the needs of very small thicknesses and the capability to resist to overpressures present inside the detectors due to the $CO_2$ gas flowing. After tests, silicon glue was selected to glue the windows on their steel frames. Typical dimensions of the windows are $2.5 \times 0.8$ m$^2$. They were tested for over and under pressure, and broke at the pressure difference, $|\Delta P| = |P_{in} - P_{atm}| = 117$ mbar. The volume of the Cherenkov box is $V_e = 2780$ l for the electron arm and $V_h = 1849$ l for the hadron arm.

When a particle crosses the Cherenkov detector, it will go through: *i)* the entrance and exit windows, for a total contribution of $5.8 \times 10^{-4}$ radiation lengths (r.l.); *ii)* the gas medium, for a total contribution of $8.2 \times 10^{-3}$ r.l.; *iii)* one mirror for about $5.5 \times 10^{-3}$ r.l. in average.

The total radiation length for the whole Cherenkov detector is $\sim 1.4 \times 10^{-2}$ radiation lengths, which is equivalent to 5 mm of typical scintillator.

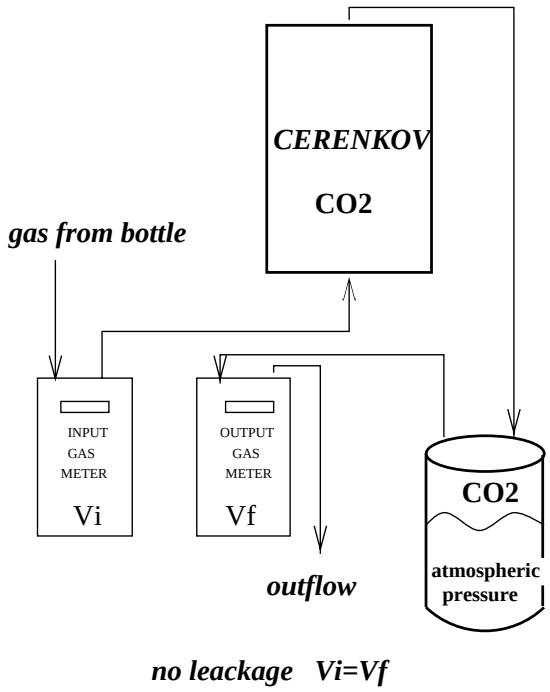


Fig. 5. Schematic description of the gas flow system.

### *3.2 The Gas System*

To ensure the gas purity, we adopted the gas flow mode of operation. A schematic description of the gas flow system is reported in Fig. 5. Since the counter will be operated at atmospheric pressure, we need to provide a small overpressure with a gas flow estimated to be $\sim$ 20 l/h. Two observations are in order: *i)* a good diagnostic procedure for gas leakage shall be provided; *ii)* air entrance from the exhaust due to a rapid change of the room temperature or atmospheric pressure in the hall shall be prevented.

The first point is solved with the installation of a pair of gas meters, recording both entrance and exit gas flow. Comparison between the entrance and exit volume recorded over several days gives a leakage diagnostic of about 1% accuracy.

For the second issue, a flexible vessel (symbolised by a cylinder in Fig. 5) is connected to the gas exit of the Cherenkov box. This vessel is able to store up to 200 l of gas ($\sim$ 10% of the total volume of the Cherenkov box) and will return it to the Cherenkov box if needed. In addition, a two-way safety valve placed on the top of the Cherenkov box, ensures that the pressure difference never exceeds $|\Delta P|_{max} = 6$ mb. This maximum value was chosen such that the window bending remains compatible with the space available between the Cherenkov detector and the other elements of the detector package. A simulation based on local atmospheric pressure data showed that the pressure

difference in absolute value will never exeed 6 mb, so that we are confident that the safety valve will hardly come into operation because of this small local variation of pressure. The data for that simulation come from the National Data Center of North Carolina and were recorded hour by hour during several years.

### *3.3 Mirrors*

The gas Cherenkov counter is positioned between other focal plane detectors. One requirement is, therefore, to influence as less as possible the properties of incoming particles. Multiple scattering and energy loss can be minimized by choosing materials with low atomic numbers and minimum thickness. The required rigidity of the whole structure has to be assured.

We have developed a relatively simple and non-expensive technique to build very light weight spherical mirrors.

Leaving the details of the employed technique of construction of the mirrors to a forthcoming paper [8], we will only summarize here their main features.

The spherical mirrors, have a radius of curvature of 90 cm. Their shape is such that their projection onto a planar surface, is a rectangle of $38 \times 48$ cm$^2$. The mirrors have been constructed with a rigid backing made of a sandwich of phenolic honeycomb between two triple layers of about 60 $\mu$m thick carbon fiber mat (180 $\mu$m on each side) glued with epoxy resin. As a support to the vacuum aluminization, 1 mm thick plexiglass sheets have been glued on the composite structure.

The phenolic honeycomb that has been employed is not the conventional (and cheeper) one with hexagonal cells. In fact, while the conventional one can be bended easily along one direction, it doesn't follow, in a natural way, the bidimensional spherical curvature. The one we have used, has cells suitably shaped to allow this kind of deformation, the cell density being 50 inch$^{-2}$.

The carbon mat has a structure with fibers randomly placed, not woven. Such a structure is homogeneus and has shaping properties better than the conventional web. It is very light and has a relatively high rigidity.

The plexiglass sheets were chosen as support of the reflecting surface, as a compromise between the required surface quality and the necessity to have a mirror as "light" as possible. Sheets of 1 mm thickness, now commercially available, were used. Their reflectivity after vacuum aluminization, measured by optical tests, is reported in Fig. 6. The results are very close to those obtained with aluminized glass [8].

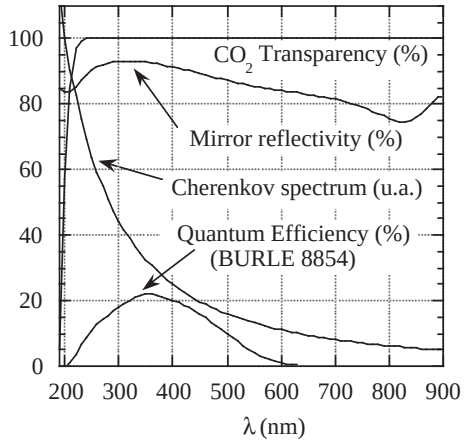


Fig. 6. Quantum efficiency $QE(\lambda)$, $CO_2$ transparency $T(\lambda)$, mirror reflectivity $R(\lambda)$ and Cherenkov radiation distribution $S(\lambda)$ (in arbitrary units) curves as functions of the wavelength $\lambda$.

The final mirror has a total average thickness of about 230 mg/cm$^2$, corresponding to about $\sim 5.5 \times 10^{-3}$ radiation lengths, better than what we could find in the literature for these kind of uses.

### *3.4 Choice of the Photomultiplier tubes and their calibration procedure with a light source.*

In threshold Cherenkov counters it is helpful to have a good identification for single photoelectron peak in the ADC spectrum. For that reason we used *Quantacon* type PM's.

BURLE has developed a high gain gallium phosphide dynode which, used as the first stage in a conventional copper beryllium multiplier chain, greately improves the PM's single photoelectron (*p.e.*) pulse height resolution. Five inches diameter BURLE 8854 PM's [9] have been chosen as a good compromise between performances and cost. The bialkali photocathode with UV-transmitting glass window has a quantum efficiency of 22.5% at 350 nm, and an enhanced sensitivity at small wavelengths (see Fig. 6).

The same PM's have been used also for the aerogel Cherenkov detector of Hall–A, and an optimization procedure of the chain resistor was carried out, as described in ref. [2]. The optimized configuration with high photocathode-to-first-dynode voltage has been adopted with a 600 k$\Omega$ resistor between the HV lead and the first dynode, while 100 k$\Omega$ resistors are employed between dynods in the rest of the chain.

The method described in ref. [10] was followed to calibrate in term of number of *p.e.*'s the PM response. The distribution of the number $n$ of *p.e.* from a

pulsed source of light follows the Poisson statistics:

$$P(n;\mu) = \frac{\mu^n e^{-\mu}}{n!} \tag{3}$$

where $\mu$ is the mean number of *p.e.* collected by the first dynode.

The final response function of the PM is then obtained taking into account the amplification effect, its spread and different sources of background. The events with $n$ *p.e.* are smeared into a gaussian with standard deviation $\sigma_n = \sqrt{n} \times \sigma_1$ being $\sigma_1$ the width of the gaussian obtained from single *p.e.* emission. For zero *p.e.* events, the ADC *pedestal* is simulated by a narrow gaussian with $\sigma_0$ width plus an exponential tail on its right-side due to background contributions (see [10] for details). To reproduce the PM response function we have used the following function:

$$\begin{aligned} R_{real}(x) = & \left\{ \frac{1-w}{\sigma_0\sqrt{2\pi}} \exp\left(-\frac{(x-Q_0)^2}{2\sigma_0^2}\right) + w\,\theta(x-Q_0)\,\alpha\,\exp\left(-\alpha(x-Q_0)\right) \right\} e^{-\mu} + \\ & + \sum_{n=1}^{\infty} \frac{\mu^n e^{-\mu}}{n!} \times \frac{1}{\sigma_1\sqrt{2\pi n}} \exp\left(-\frac{(x-Q_0-Q_{sh}-nQ_1)^2}{2n\sigma_1^2}\right) \end{aligned} \tag{4}$$

where $Q_0$, $\sigma_0$ (position and width of the *pedestal*), $w$, $\alpha$ (parameters for the background in the right-side tail of the pedestal), $Q_1$, $\sigma_1$ (distance between two adjacent gaussians and width of the one-*p.e.* gaussian, respectively) and, finally, $\mu$ (the mean number of *p.e.*) are seven "free" parameters. $Q_{sh} = w/\alpha$ is the effective spectrum shift due to background, $\theta(x - Q_0) = 0$ if $x < Q_0$, $\theta(x - Q_0) = 1$ elsewhere.

Being $n$ the number of *p.e.* and considering the Poisson weighting factor $P(n;\mu)$ when $n$ *p.e.* are emitted, the above formula is in fact the sum of the following contributions:

*i)* $n = 0$ : a narrow gaussian (the pedestal) with standard deviation $\sigma_0$ at ADC channel $Q_0$ plus an exponential tail accounting for the background;

*ii)* $n = 1$ : a gaussian with standard deviation $\sigma_1$ at ADC channel $Q_0$+$Q_{sh}$+$Q_1$;

*iii)* $n > 1$ : gaussians with standard deviation $\sigma_n = \sqrt{n} \times \sigma_1$ far from the $(n-1)th$ peak by $Q_1$ channels;

For the calibrations, we have used a pulsed source of light peaked at a wavelength of 490 nm. The amplitude and time-length (min. 10 ns) of the light pulses could be adjusted. The spectra obtained under different circumstances

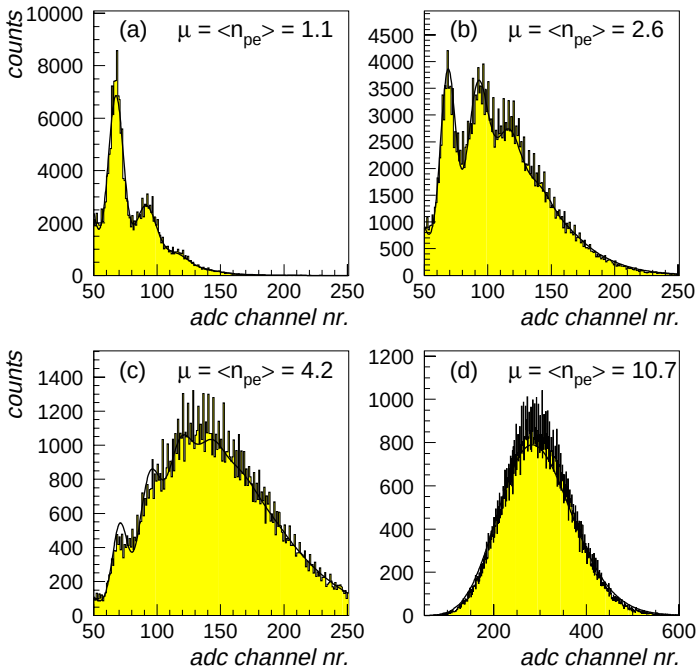


Fig. 7. Calibrations of a BURLE 8854 PM response made with a pulsed light source with increasing amplitude. The spectra have been fitted with eq.4. The obtained parameters are reported in table 1.

have been fitted with Eq.(4). Calibration tests were performed essentially by varing the high voltage applied to the PM's and the intensity of the light source. Fig. 7 shows the spectra obtained at 2300 V with increasing intensity of the light. The resulting fits are reported with a continuous line. In the case of Fig. 7(b) all the seven parameters of the fitting function plus a normalization constant were left free. In the other three cases $Q_0$, $\sigma_0$, $Q_1$, $\sigma_1$ where kept fixed as obtained from the first spectrum (7(b)), $w$ and $\alpha$ were free in order to reproduce better the background below 1 *p.e.* peak, and $\mu$ the average number of photoelectrons has been obtained as a result of the fit. The parameters found from the fit are reported in Table 1. As can be seen the fitting function reproduce remarkably well the data. The same holds for high voltages in the range 2200 - 2500 V. At voltages higher than 2700 V, Eq. 4 does not reproduce the PM response anymore, since it looses its linearity. At these voltages, a saturation in the position of the *p.e.*'s peak has been observed in the spectra.

## 4 Calculated photoelectron yield

Defining the detection efficiency $\varepsilon$ as the probability to have for each event any number of photoelectrons emitted but zero, then the following formula

Table 1
Parameters obtained in the fit of the spectra reported in Fig. 7. The symbol (*) stands for parameters kept fixed in the fit.

| Spectrum | $Q_0$ | $\sigma_0$ | $Q_1$ | $\sigma_1$ | $w$ | $\alpha$ | $\mu =< n_{p.e.} >$ |
|---|---|---|---|---|---|---|---|
| Fig. 7(a) | 42.4 (*) | 0.6 (*) | 23.3 (*) | 6.1 (*) | 0.34 | 0.176 | 1.10 |
| Fig. 7(b) | 42.4 | 0.6 | 23.3 | 6.1 | 0.36 | 0.119 | 2.62 |
| Fig. 7(c) | 42.4 (*) | 0.6 (*) | 23.3 (*) | 6.1 (*) | 0.50 | 0.098 | 4.24 |
| Fig. 7(d) | 42.4 (*) | 0.6 (*) | 23.3 (*) | 6.1 (*) | 0.30 | 0.07 | 10.74 |

holds:

$$\varepsilon = 1 - e^{-\mu} \tag{5}$$

where $\mu$ is the mean number of photoelectrons collected by the first dynode as determined from the PM spectrum.

The spectrum shape, and $\mu$, can be evaluated by a Monte Carlo simulation. The following steps have been followed for each particle (electrons at 2 GeV/c) crossing a length $L$ of radiator:

*i)* the number of emitted photons (per event) $n_\gamma$ is generated in the range of wavelengths from $\lambda_1 = 200$ nm to $\lambda_2 = 700$ nm, according to the range detectable by the used PM. $n_\gamma$ is chosen as a random number in a Poisson statistics with mean value:

$$N_\gamma = 2\pi\alpha L \sin^2\theta_C \left(\frac{1}{\lambda_1} - \frac{1}{\lambda_2}\right) \tag{6}$$

*ii)* The wavelength $\lambda$ of each of the $n_\gamma$ photons is chosen as random number following the Cherenkov distribution $1/\lambda^2$ (see the Cherenkov radiation curve in Fig. 6). The probability to be transmitted through the radiator and to be reflected from the mirror (i.e. to be not absorbed), are accounted for by the transmittivity $T(\lambda)$ and reflectivity $R(\lambda)$ curves also reported in Fig. 6.

*iii)* The photons arriving to the PM succeed to undergo to photoelectric effect on the photocathode by comparing a random number with the quantum efficiency curve reported in Fig. 6.

The "ideal" distribution of photoelectrons so obtained, is reported in Fig. 8(a). The "real" response of the photomultiplier is obtained by folding the events of Fig. 8(a) with gaussians of width $\sigma_n$ as explained before. The values of the parameters $Q_0$, $\sigma_0$, $Q_1$, $\sigma_1$, $Q_{sh}$ (see formula (4)) are obtained from the

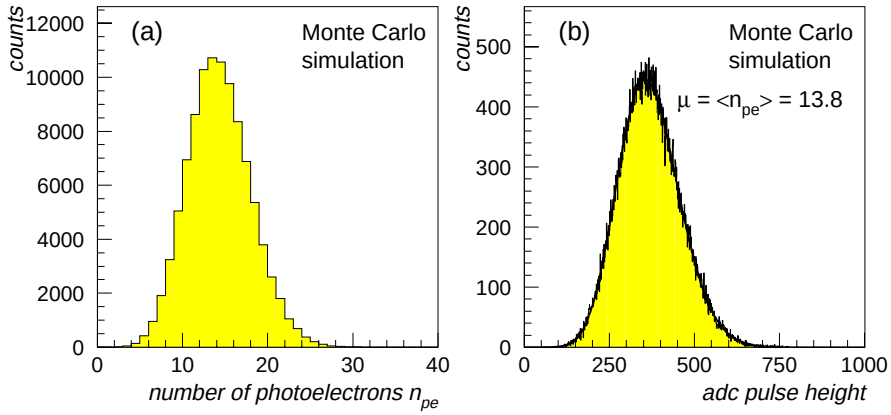


Fig. 8. Distribution of photoelectrons as obtained from a Monte Carlo simulation *(a)*, and the simulated ADC "real" response *(b)*. An average number of 13.8 *p.e.* has been obtained from the fit of the ADC pulse height distribution.

calibration procedure of §3.4 and kept fixed (see table 1). The obtained "real" spectrum is then fitted with the formula (4) in order to extract the mean number of produced photoelectrons $\mu$ and thus the detector efficiency $\varepsilon$.

The result is shown in Fig. 8(b). The expected mean number of produced photoelectrons is $\mu =< n_{p.e.} >= 13.8$ per meter, resulting in a theoretical detection efficiency of practically 100%. The figure of merit of the detector is than predicted to be $N_0 = 168$ cm$^{-1}$. This fit is checked to be consistent with the distribution reported in Fig. 8(a).

## 5 Test and performance of the Cherenkov detector prototype

The prototype counter, shown in Fig. 9, is a full-sized reproduction of one single section of the final detector. It has one channel (one mirror, one PM) with a radiator effective length of 1 m.

The tests have been carried out at CERN, where conditions similar to those at Jefferson Lab are obtainable. A mixed beam of positrons, pions and protons with momenta in the range 1 to 4 GeV/c ($\pm$1.3% of momentum resolution) has been used in the T10 test area of the PS [11]. With such a beam it has been possible to evaluate the efficiencies for positrons, as well as the rejection ratios for pions and protons.

The event trigger was generated by a triple coincidence of three finger plastic scintillators placed upstream, just in front of the counter and downstream, respectively. The distance between the first and the last scintillators was about 20 m. A veto paddle to avoid pile-up effects with particles from the halo of

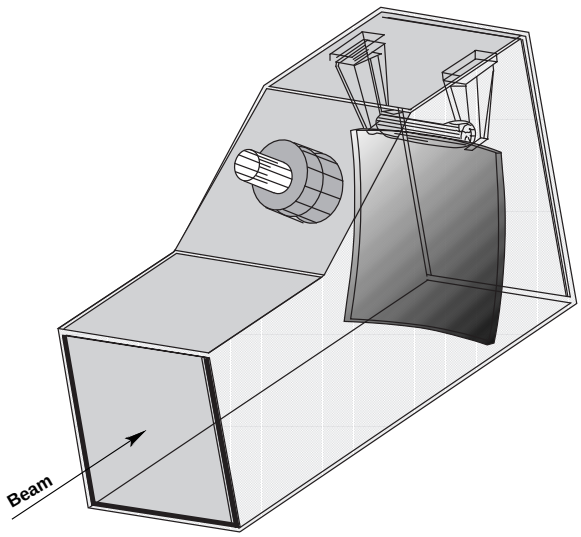


Fig. 9. Prototype of the Gas Cherenkov Detector.

the beam, was also included in the trigger system. To isolate the contributions of positrons, pions and protons on an event by event basis, the information from two Cherenkov detectors placed on the beam line, operating with $CO_2$ in pressure available in the T10 experimental hall have been employed, in combination with the time of flight (TOF) technique. In Fig. 10 an example of the identification of 2 GeV/c momentum particles is shown. In the figure, only the selection through the TOF and the signal from one gas Cherenkov of the beam line, is reported. In the analysis of the data, the additional information from the second gas Cherenkov detector is also used to further reduce (to the level of $10^{-5}$) the probability of a wrong identification of the particles.

### *5.1 Average number of photoelectrons*

As a first step in understanding the performances of the detector under beam measurements, the average number of photoelectrons has been evaluated. A beam of 2 GeV/c has been used, positrons have been selected and the response of the PM operating at 2300 V has been studied.

Fig. 11 shows the resulting spectrum and the result of the fit of Eq. 4. The fit has been performed with only two free parameters: the normalization constant and the average number of *p.e.*. All the other parameters (intrinsic to the PM properties, not depending on the physical process) were kept fixed as obtained from the calibrations in §3.4 and taken from Table 1. From the fit, an average number of *p.e.* $\mu = 9.0$ has been estimated. Such a number has to be compared with the theoretical value $N_{pe}^{theor} = 13.8$ found with the Monte Carlo simulation in the previous chapter. A reduction of about 30 % has been observed which is within the expectations based on what can be found in

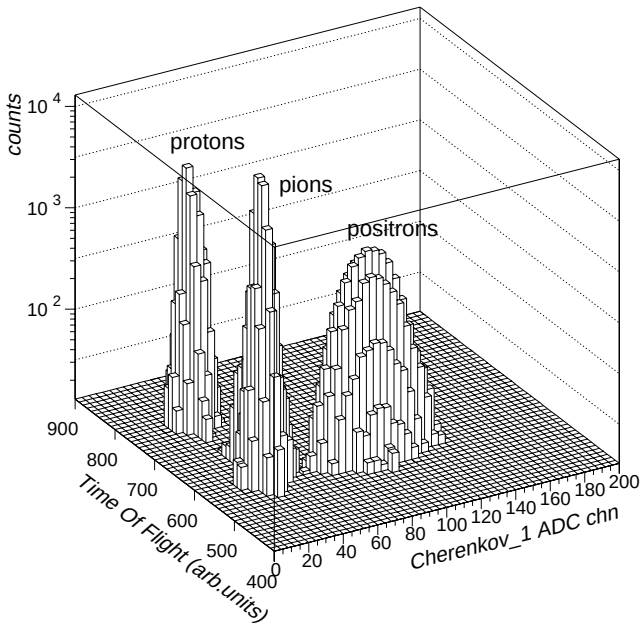


Fig. 10. Particle Identification for the test of the prototype Cherenkov detector performed at CERN.

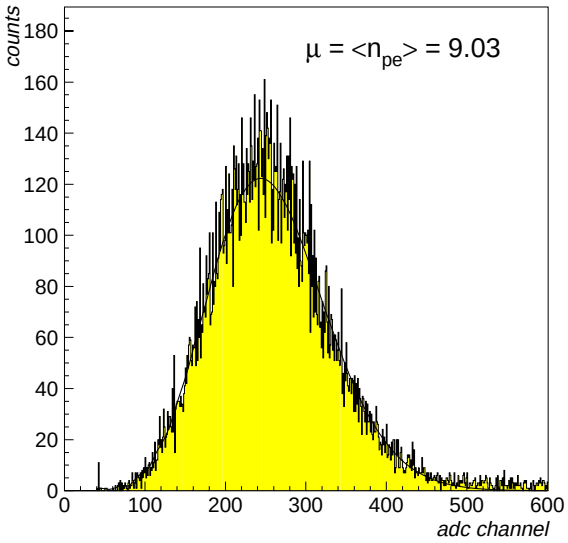


Fig. 11. Pulse-height spectrum obtained with 2 GeV/c positrons. The fitting procedure described in the text shows a production of 9.0 *p.e.*.

literature (see e.g. Ref. [12]).

As can be seen from Fig. 6, the spectral sensitivity in the UV region of the chosen PM decreases below 300 nm. In order to make use of the $1/\lambda^2$ increase of the Cherenkov photon emission, a greater sensitivity to shorter wavelength

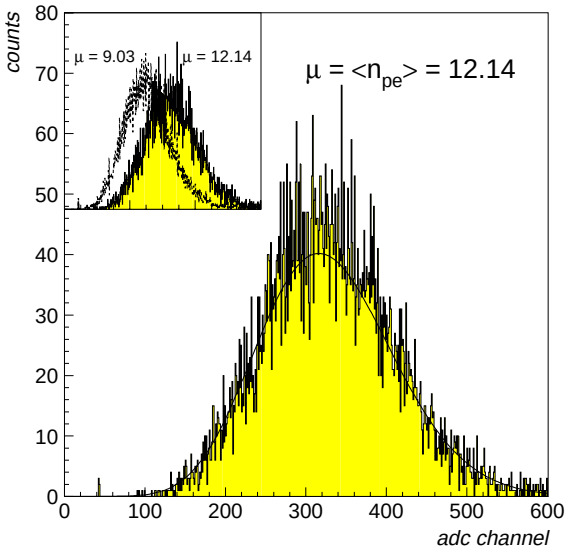


Fig. 12. Pulse-height spectrum obtained with 2 GeV/c positrons with a p-terphenyl coated PMT. The fitting procedure described in the text shows a production of 12.1 *p.e.*. For comparision, the shapes obtained with and without wavelength shifter (filled and empty histograms, respectively) are also reported in the figure.

would be helpful. To enhance the UV sensitivity of the PM, we have coated the glass window with a wavelength shifter [13]. A thin layer ($\sim$ 0.8 $\mu$m) of p-terphenyl ($C_{18}H_{14}$) has been evaporated onto the glass window of the PM. Its maximum absortion being at $\sim$ 270 nm with a re-emission around 350 nm where the quantum efficiency of ours PM's reach a maximum. The result obtained with such a coated PM is reported in Fig. 12. An average yield of 12.1 *p.e.* has been measured giving $N_0 = 147$ cm$^{-1}$ as figure of merit, an improvement of about 34% compared to the not coated tubes.

### *5.2 $e^+$ detection efficiency and $p, \pi^+$ contamination (rejection)*

A typical ADC response of the Cherenkov detector with a terphenyl coated PM is shown in Fig. 13 (a) for undistinguished particles of 2 GeV/c, and in Figs. 13 (b,c,d) where positrons, pions and protons have been separated through the TOF and the two gas Cherenkov of the beam line.

The efficiencies to detect a given particle as a function of the software threshold chosen in the ADC response have been deduced from the spectra of Figs. 13 (b,c,d), in the case of a 2 GeV/c beam, and from analogous spectra measured for other momenta. Once a software cut is put at channel $N_{thr}$, the efficiency is defined as the sum of counts above $N_{thr}$ divided by the total

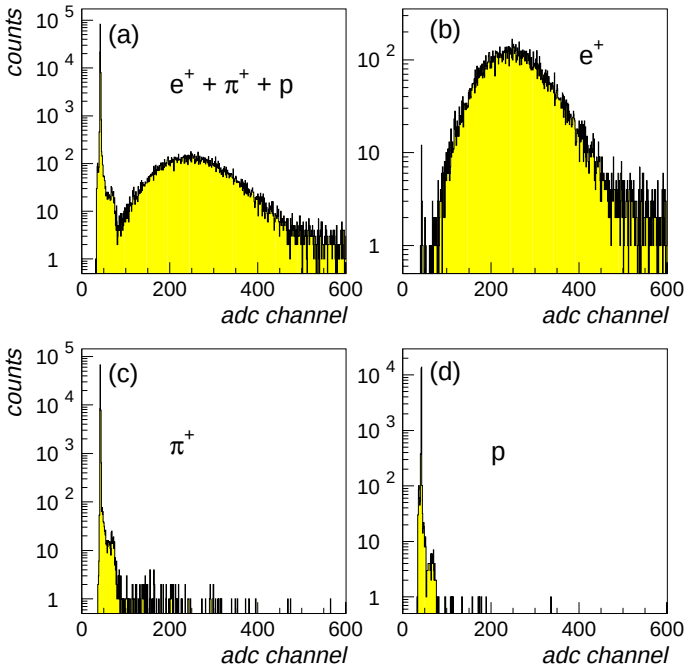


Fig. 13. Pulse-height spectra obtained with a 2 GeV/c beam: (a) no selection applied; (b) positrons selected; (c) pions selected; (d) protons selected.

number of counts in the spectrum:

$$\varepsilon(N_{thr}) = \sum_{i>N_{thr}} counts(i)/N_{TOT}$$

.

We report in Fig. 14 the efficiencies obtained for pions and protons (in this case intended as *contaminations*) together with the *inefficiencies* $(1-\varepsilon)$ for positrons measured at 2, 3 and 4 GeV/c.

If a cut is applied to have at least a production of 2 photoelectrons, an inefficiency for positrons less than $10^{-3}$ has been measured at all momenta. With the same cut, the contamination for protons (and hence the rejection ratio $p/e$) is always lower than $10^{-3}$ and the contamination for pions (the rejection ratio $\pi/e$) is about $2 \times 10^{-3}$ at 2 and 3 GeV/c. A higher pion contamination has been measured at central momenta of 4 GeV/c, dropping to less than $4 \times 10^{-3}$ for $n_{p.e.} > 4$.

Neglecting the scintillation, the detected contaminations for particles below the Cherenkov threshold come essentially from two contributions : *i)* accidental background, coming from different sources (essentially PM dark current and beam related noise); *ii)* detection of Cherenkov light produced by energetic

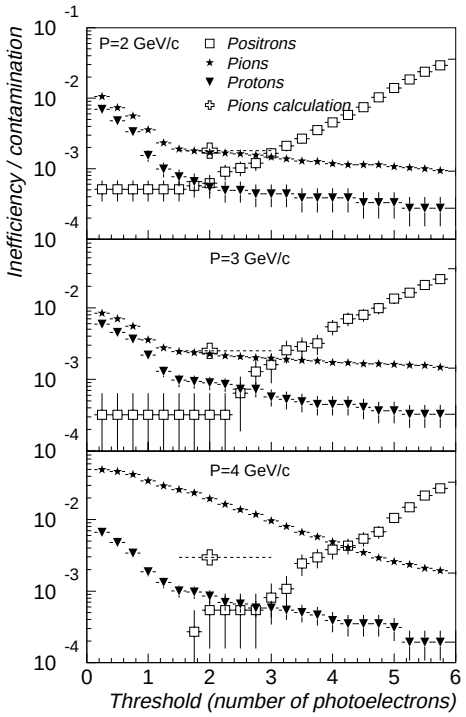


Fig. 14. Positrons inefficiencies and contaminations for pions and protons, measured, and $\delta$-rays computed contribution from pions, at 2,3 and 4 GeV/c in CERN test conditions.

knock-on electrons ($\delta$-rays).

While for pions the production of energetic knock-on electrons is the dominant contribution, this effect is absent for protons in the measured range of momenta, since in this case protons are not fast enough to produce secondary electrons above the Cherenkov threshold ($p_{thres}^{electron} = 17.34$ MeV/c in $CO_2$ at STP). This explains why we observe "efficiencies" which are higher for pions than for protons. The detected proton contamination has been interpreted as accidental background as it was found consistent with off time ADC gate measurements.

### *5.2.1 Production of energetic knock-on electrons ($\delta$ rays)*

In order to understand the contaminations for particles below the Cherenkov threshold due to the $\delta$-rays production, a code has been developed and adapted to our specific conditions. The formula for the $\delta$-rays yield per g/cm$^2$ has been taken from the GEANT manual [14]. The contribution from all the different sources of materials placed upstream the mirror of the Gas Cherenkov detector have been taken into account with the following selections : *i)* regardless to the source, a minimum number of *p.e.* $n_{pe}$ must be produced (e.g. setting a

threshold to $n_{p.e.} \geq 2$, can discard delta energies very close to the Cherenkov threshold); *ii)* depending on the source, the delta rays must cross the mirror: this set a maximum delta production angle and obviously sources closer to the detector will contribute much more; *iii)* depending on the source, the scattered primary particle must produce a trigger: this set a maximum primary particle scattering angle; *iv)* the impact angle of the knock-on electron to the mirror is limited by the angular acceptance of the photocathode.

In our specific case, conditions *ii)* and *iii)* imply that the knock-on electron particles always have momenta much bigger than the threshold momentum ($p \gg p_{thres} = 17$ MeV/c), so that they always produce a number of photo-electron very close to that of ultrarelativistic particles. In practice, this means that from condition *i)*, there is no variation in the $\delta$-rays production yields with different cut on $n_{pe}$, when $n_{pe}$ is low.

Results for pions of 2, 3 and 4 GeV/c in CERN calibration conditions and for $n_{p.e.} \geq 2$ are reported in Table 2 and also plotted in Fig. 14. As can be seen, the calculated $\delta$-rays production yields per pion are in very good agreement with the contamination of pions obtained at 2 and 3 GeV/c. In the case of 4 GeV/c some disagreement is found in the low *p.e.* part of the data where the contamination of pions seems to be due to other effects that sum up to the $\delta$-rays production. In that case it must be pointed out that the "nominal" Cherenkov threshold for pions in $CO_2$ at STP is $\sim$4.8 GeV/c but the threshold could be lower $\sim$4.3 GeV/c in our case where an overpressure of about 0.2 bar was present in the detector. Moreover, the combination of momentum calibration in the beam line and the momentum acceptance could be the cause of having pions just above the Cherenkov threshold, giving a number of *p.e.* significantly lower than the positron peak. The contamination drops to values in agreement with the $\delta$-rays production yield for $n_{pe} > 4$.

## 6 Summary and conclusions.

Two atmosferic pressure $CO_2$ gas Cherenkov detectors for electron-pion separation have been built for the hadron and for the electron arms of the two High Resolution Spectrometers for the Hall–A of the CEBAF facility at Jefferson Lab. The two detectors match all the geometrical and functionality needs of Hall–A [1].

The mirrors have been built at our laboratories following the requirement to be as "thin" as possible to minimize multiple scattering and energy loss of the incoming particles. Spherical shells mirrors have been produced with a total average thickness of about $5.5 \times 10^{-3}$ radiation length, which is the thinnest, to our knowledge, for mirrors built for these uses.

Table 2
Computed above threshold $\delta$-rays production yields from a pion of 2, 3 and 4 GeV/c. The partial contribution of each material placed upstream the mirror is reported.

| CH equivalent thickness ($g/cm^2$) | distance from the mirror (m) | $\delta$-rays yield (per pion) @ p=2 GeV/c | $\delta$-rays yield (per pion) @ p=3 GeV/c | $\delta$-rays yield (per pion) @ p=4 GeV/c |
|---|---|---|---|---|
| 1.0 | 5.0 | $1.50 \times 10^{-5}$ | $2.50 \times 10^{-5}$ | $3.40 \times 10^{-5}$ |
| 2.0 | 2.8 | $2.00 \times 10^{-4}$ | $3.20 \times 10^{-4}$ | $4.00 \times 10^{-4}$ |
| 2.3 | 2.1 | $5.98 \times 10^{-4}$ | $8.28 \times 10^{-4}$ | $1.01 \times 10^{-3}$ |
| 1.7 | 1.32 | $9.18 \times 10^{-4}$ | $1.22 \times 10^{-3}$ | $1.39 \times 10^{-3}$ |
| 0.15 | 0.6 | $8.10 \times 10^{-5}$ | $1.08 \times 10^{-4}$ | $1.23 \times 10^{-4}$ |
| Total yields | | $1.81 \times 10^{-3}$ | $2.51 \times 10^{-3}$ | $2.96 \times 10^{-3}$ |

Tests performed at CERN with a prototype counter have shown that ultra-relativistic particles in 1 meter of $CO_2$ at about 1.1 bar produce an average number of photoelectron $n_{pe} = 9.0$ with the use of BURLE 8854 phototubes, about 65% of the expected value. An improvement of $\sim$ 34% on $n_{p.e.}$ has been obtained through the use of the p-terphenyl wavelength shifter coated onto the glass window of the photomultiplier, resulting in an average yield of photoelectron $n_{pe} = 12.1$ and a figure of merit $N_0 = 147$ cm$^{-1}$.

The performances of the full-sized prototype of a single section of the Cherenkov counters, has clearly shown the capability to have a good electron identification and hadron component discrimination as required for the Hall–A performances [1].

The detection efficiencies for positrons, pions and protons for central momenta of 2, 3 and 4 GeV/c have been reported in this paper. When a reasonable threshold is applied (above 2 photoelectrons) an inefficiency for positrons less than $10^{-3}$ has been measured at all momenta. With the same cut, the contamination for pions (and hence the rejection ratio $\pi/e$) was about $2 \times 10^{-3}$ at 2 and 3 GeV/c in CERN test conditions, in very good agreement with the computed yield of energetic knock-on electrons ($\delta$-rays production) at these momenta. A higher contamination of few $10^{-2}$ has been measured at "nominal" central momenta of 4 GeV/c, in disagreement with the calculation. A possible explanation of this result is given in the last section.

The proton contamination, for which $\delta$-rays cannot contribute, was measured to be less than $10^{-3}$, consistent with accidental background measurements.

## References


[1] CONCEPTUAL DESIGN REPORT, Southern University Research Association (SURA), CEBAF, Newport News, Virginia, April 1990.

[2] L.Alexa et al., *Nucl. Instrum. Methods* A **365**, 299 (1995).

[3] G.Lolos et al., *Nucl. Instrum. Methods* A **385**, 403 (1997).

[4] P.Markowitz et al., CEBAF Technical Note TN 94-034, Sept. 1994.

[5] S.Kowalski and H.A.Enge, "RAYTRACE Users Manual", LNS/MIT, May 1986.

[6] P.Vernin, computer code "SNAKE", unpublished.

[7] P.Vernin, computer code "MIRROR", unpublished.

[8] E.Cisbani et al., paper in preparation.

[9] Burle 8854 5-in. 14-stage Quantacon photomultiplier made by Burle Industries Incorporated, 1000 New Holland Avenue, Lancaster, PA 17601, USA.

[10] Bellamy et al., *Nucl. Instrum. Methods* A **339**, 468 (1994).

[11] K.Batzner, D.Dumollard, L.Durieu, D.J.Simon, F.Cataneo, and M.Ferro-Luzzi, CERN PS/PA-EP Note 88-26.

[12] Biino et al, *Nucl. Instrum. Methods* A **235**, 488 (1985).

[13] G.Eigen and E.Lorentz, *Nucl. Instrum. Methods* **166**, 165 (1979), E.L.Garwin et al., *Nucl. Instrum. Methods* **107**, r3165 (1973).

[14] GEANT User's Guide, GEANT 3, CERN Program Library Long Writeup W5013.